Tectonophysics 674 (2016) 135–146

Contents lists available at ScienceDirect

Tectonophysics

journal homepage: www.elsevier.com/locate/tecto

# Strong Lg-wave attenuation in the Middle East continental collision orogenic belt

Lian-Feng Zhao [a,*], Xiao-Bi Xie [b]

[a] Key Laboratory of Earth and Planetary Physics, Institute of Geology and Geophysics, Chinese Academy of Sciences, Beijing 100029, PR China
[b] Institute of Geophysics and Planetary Physics, University of California at Santa Cruz, CA, USA

ARTICLE INFO

*Article history:*
Received 15 December 2015
Received in revised form 10 February 2016
Accepted 15 February 2016
Available online 27 February 2016

*Keywords:*
Lg attenuation
Q tomography
Continental collision orogenic belt
The Middle East

ABSTRACT

Using Lg-wave Q tomography, we construct a broadband crustal attenuation model for the Middle East. The $Q_{Lg}$ images reveal a relationship between attenuation and geological structures. Strong attenuation is found in the continental collision orogenic belt that extends from the Turkish and Iranian plateau to the Pamir plateau. We investigate the frequency dependence of $Q_{Lg}$ in different geologic formations. The results illustrate that $Q_{Lg}$ values generally increase with increasing frequency but exhibit complex relationships both with frequency and between regions. An average $Q_{Lg}$ value between 0.2 and 2.0 Hz, $Q_{Lg}$ (0.2–2.0 Hz), may be a critical index for crustal attenuation and is used to infer the regional geology. Low-$Q_{Lg}$ anomalies are present in the eastern Turkish plateau and correlate well with low Pn-velocities and Cenozoic volcanic activity, thus indicating possible partial melting within the crust in this region. Very strong attenuation is also observed in central Iran, the Afghanistan block, and the southern Caspian Sea. This in line with the previously observed high crustal temperature, high-conductivity layers, and thick marine sediments in these areas, suggests the high Lg attenuation is caused by abnormally high tectonic and thermal activities.



## 1. Introduction

The Middle East continental collision orogenic belt is the consequence of the ongoing northward convergence of the African, Arabian and Indian plates towards Eurasia (Fig. 1). During different geological ages, continent-continent collisions created the Anatolian, Turkish, Iranian, Pamir and Tibetan plateaus with a sinuous boundary (e.g., Yin, 2010). The Indian-Eurasian collision initiated in the Paleocene to Middle Eocene (65–45 Ma) (e.g., Yin and Harrison, 2000; Yin et al., 2002), and the Arabian and Eurasian plates collided between the Late Eocene and Middle Miocene (40–13 Ma) (Allen and Armstrong, 2008; Berberian and King, 1981; Dewey et al., 1986; Sengör and Kidd, 1979; Yin, 2010). The oceanic African plate continues to subduct beneath the Eurasian plate under the present-day Mediterranean sea (Jolivet and Faccenna, 2000). The collision tectonics were dominated by the Paleotethys closure in Middle Triassic times, the closing of the Neotethys ocean, and subsequent tectonic processes, e.g., the subduction of oceanic plates, large-scale transform faulting, compressional mountain building and crustal extension (e.g., Agard et al., 2005; Stampfli, 2000). These complex tectonic processes are usually accompanied by thermal activity, which strongly affects the material properties and behavior of individual geological blocks (geo-blocks).

Seismic attenuation is usually an indicator of high temperature and partial melting in the Earth's interior. Recently, we obtained a broadband Lg-wave attenuation model for the Tibetan plateau, which depicts areas with thermal anomalies, and suggested that within the Tibetan crust, there exist two material flow channels that might be responsible for the observed strong Lg-wave attenuation (Zhao et al., 2013a). To the west of the Tibetan plateau, with an adjacent orogenic belt, the Turkish and Iranian plateau is a young and geologically active continental collision zone (Dewey et al., 1986). Strong seismic attenuation in the continental collision belt has been observed by previous investigators (Al-Damegh et al., 2004; Bao et al., 2011b; Cong and Mitchell, 1998; Gök et al., 2003; Kadinsky-Cade et al., 1981; McNamara and Walter, 2001; Pasyanos et al., 2009; Rahimi et al., 2010; Rodgers et al., 1997; Sandvol et al., 2001; Zor et al., 2007). Sandvol et al. (2001) measured the relative attenuation from Lg/Pg amplitude ratios in the Middle East. Al-Damegh et al. (2004) used a larger dataset to image the Lg/Pg propagation efficiency. They found inefficient or blocked Lg propagation within the continental collision zones and relatively efficient propagation in the stable Arabian plate. Zor et al. (2007) observed very low $Q_0$ values ($Q_{Lg}$ at 1 Hz) of approximately 100–200 in the Anatolian plateau and suggested that these values indicate tectonic complexity and widespread crustal melting. Pasyanos et al. (2009) modeled broadband Lg attenuation in the Middle East and found that the continental collision

* Corresponding author at: Key Laboratory of Earth and Planetary Physics, Institute of Geology and Geophysics, Chinese Academy of Sciences, 19 Beituchengxilu, Chaoyang district, Beijing, PR China, 100029. Tel.: +11 86 10 82998658; fax: +11 86 10 62010846.
*E-mail addresses:* zhaolf@mail.iggcas.ac.cn (L.-F. Zhao), xxie@ucsc.edu (X.-B. Xie).

http://dx.doi.org/10.1016/j.tecto.2016.02.025

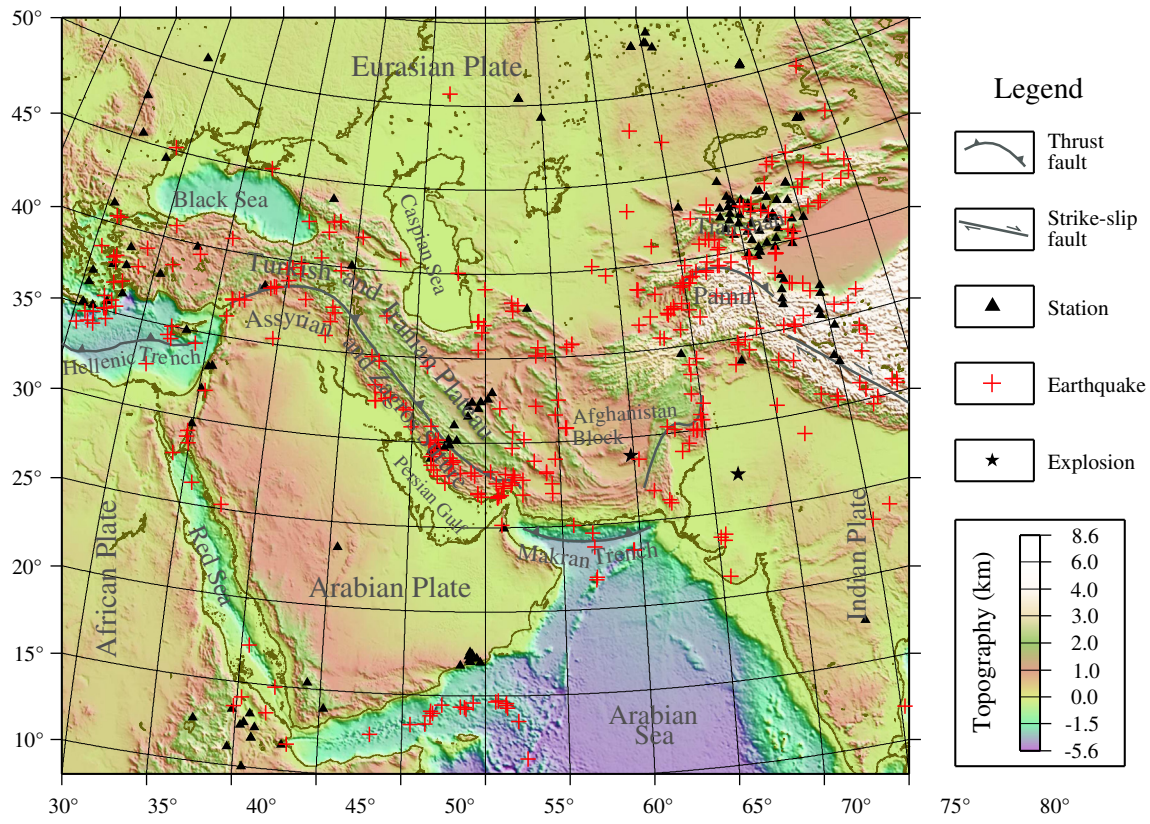


**Fig. 1.** A topographic map that shows our study area overlaid with the major faults (black lines) that indicate the continental collision boundary, the station locations (triangles) and the event epicenters for the selected earthquakes (red crosses) and nuclear explosions (stars) used in this study. Also labeled on the map are the names of the major geo-blocks and faults.

orogenic belt has relatively lower Q values at individual frequencies, whereas the Q values are much greater in stable plates. Compared with the Tibetan plateau, no great elevation drives gravity flow within the crust in the Turkish and Iranian plateau (Copley and McKenzie, 2007). However, because of the continental collision, there still is relatively high topography in this region. Thus, the potential gravitational energy, along with the lateral extrusion in the orogens, possibly drives the crustal material flow. Both the widespread partial melting and possible crustal flow significantly link the seismic attenuation and dynamic processes in the Middle East (Vanderhaeghe and Teyssier, 2001; Zhao et al., 2013a; Zor et al., 2007).

In this study, we use regional seismic data to develop a high-resolution Lg-wave attenuation model in the Middle East and adjacent regions, explore the relationship between crustal attenuation and regional tectonics, and infer the thermal activity in the lower crust and upper mantle.

## 2. Regional wave data set

The Lg waveform dataset used in this study consists of 6158 broadband vertical-component digital seismograms recorded at 144 stations from 335 regional earthquakes and 2 nuclear explosions between February 1994 and January 2013. These waveforms, which were retrieved from the Incorporated Research Institutions for Seismology consortium Data Management Center (the IRIS DMC), were selected from crustal earthquakes with magnitudes between $m_b$ 4.0 and 6.0, recorded at epicenter distances between 200 and 3000 km. The station parameters, including the code, location, sampling rate, network, data resource, and affiliation, are listed in Tables S1 and S2 in the supplementary document. These stations are equipped with broadband instruments with a nearly flat velocity response from 0.03 Hz to approximately 8.0 Hz or higher. The event parameters are listed in Table S3 in the supplementary document. Fig. 1 is a topographic map that shows the locations of the stations (triangles), earthquakes (crosses) and nuclear explosions (stars) used in this study. As illustrated in Tables S1 and S3, each station recorded at least three events, and each event was observed by at least three stations. Thus, our Lg-waveform dataset can provide better constraints on both the source spectra and site response when resolving the regional attenuation distributions.

The group velocity of the Lg phase is an important parameter in modeling the spectral amplitude (e.g., Xie and Mitchell, 1990). Because of the differences of crustal structure and uncertainties in origin times and event locations, the Lg-wave group velocities vary from region to region. Pasyanos et al. (2009) investigated bandpass-filtered seismograms and found there is an apparent difference between Lg-wave group velocities in south Iran and central Arabia. To further investigate Lg-wave group velocities, we stacked regional waveforms. Fig. 2a illustrates a vertical-component velocity seismogram recorded at the KUR station from the earthquake on 1998/05/28 (refer to Table S1), at a distance 1482.3 km, where a filter with a passband between 0.05 and 10.0 Hz is applied. The normalized waveform energy is shown in Fig. 2b. After processing all regional seismograms, we obtain a stacked energy distribution, as shown in Fig. 2c. Several distinct arrivals can be identified in the Middle East region. The first arrival is Pg at short distances, and turned into Pn at larger distances. The latter has a group velocity of 8.0 km/s. The Sn-wave is relatively weak but can be traced at most distances. It has a group velocity of 4.5 km/s. The Lg-wave has a group velocity of 3.5 km/s. Considering the uncertainties in the origin time, epicenter location, source depth, etc., we used a floating group-velocity window to extract the Lg-waveform. First, the vertical-component velocity waveforms were filtered between 0.5 and 1.5 Hz. Second, the interval for the Lg-wave group-velocity window was set to be 0.6 km/s. We then scanned the Lg-waveform within a larger window ranging from 3.7 to 2.8 km/s, and finally determined the Lg group-velocity window based on the maximum energy. Following Zhao et al.

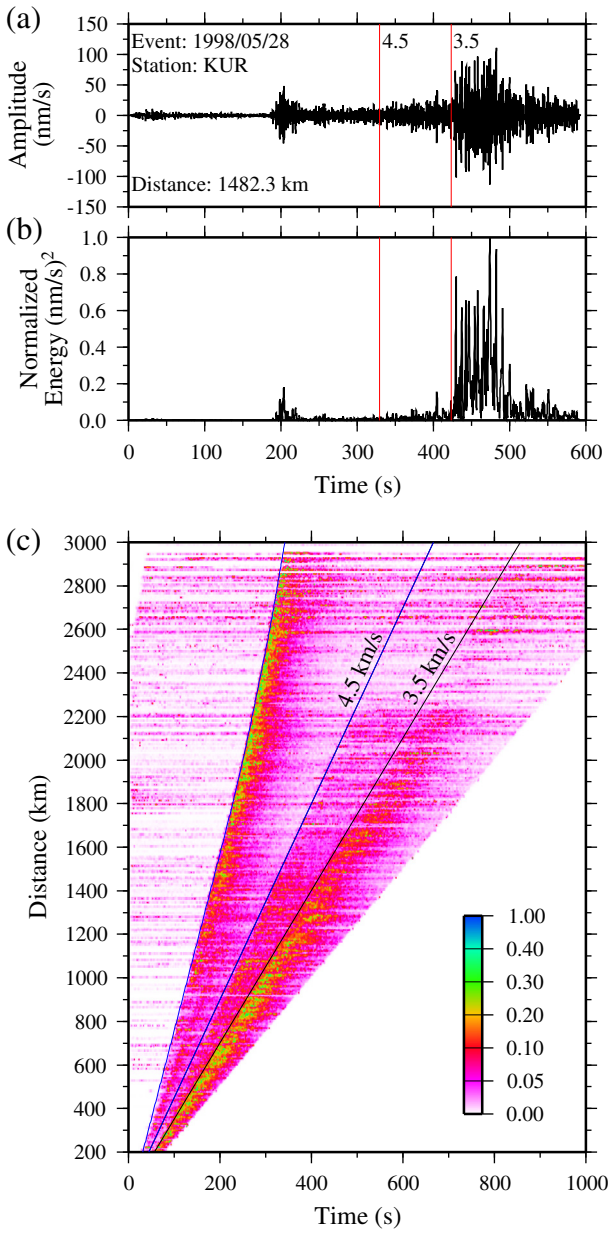


**Fig. 2.** (a) An example seismogram recorded at the station KUR, (b) its normalized waveform energy, and (c) stacked energy distribution for all regional seismograms used in this study. Also plotted in (b) and (c) are the group velocities, which are 4.5 and 3.5 km/s for the Sn- and Lg-waves, respectively.

(2010, 2013b), we picked the noise series in an equal-length time window with the Lg phase before the first-arriving P wave. The Fourier spectra were calculated for both Lg-waves and noise. We sampled the spectral amplitudes at 58 frequencies distributed log-evenly between 0.05 and 10.0 Hz and corrected for the effect of noise on the signal amplitudes (for details see Zhao et al., 2013a, 2013b). After processing all regional waveforms, we obtained source-station (single-station) amplitudes at individual frequencies within the frequency band.

Following Xie et al. (2004) and Zhao et al. (2013b), we extracted two-station data and two-event data for individual frequencies from the single-station data. The modeling of Lg-spectra for single-station, two-station, and two-event data sets is detailed in Appendix A. Based on these data sets, we conducted Lg-wave Q tomography to jointly invert the $Q_{Lg}$ distribution, Lg-wave source function, and site response in the Middle East.

## 3. Lg-wave Q tomography using single-station, two-station and two-event data sets

Both regional Lg (e.g., Benz et al., 1997; Fan and Lay, 2002; Pasyanos et al., 2009; Phillips et al., 2005; Sandvol et al., 2001; Xie et al., 2004; Zhao et al., 2013a) and Lg coda (e.g., Aki and Chouet, 1975; Cong and Mitchell, 1998; Ford et al., 2008; Mitchell et al., 1997, 2008) spectra have been used in $Q_{Lg}$ tomography. In this study we focus primarily on the Lg spectrum. According to the measurement methods used, the inversion can use a single-station method (Pasyanos et al., 2009; Pei et al., 2006; Xie, 1993; Zhao et al., 2010), a two-station method (Fan and Lay, 2002, 2003a; Xie, 2002; Xie et al., 2004, 2006; Zor et al., 2007), or mixed two-station/two-event data (Akinci et al., 1995; Bao et al., 2011a; Chun et al., 1987; Fan and Lay, 2003b; Ranasinghe et al., 2015). To reduce the tradeoffs between the attenuation and source terms, Zhao et al. (2013b) combined single- and two-station data to invert a high-resolution broadband $Q_{Lg}$ model. Following Zhao et al. (2010, 2013b) and under the specific survey system, we constructed the single-station, two-station and two-event datasets at each frequency for inversion. The single-station data have the highest ray coverage, which increases the inversion resolution. The two-station data eliminate the source function and involve less tradeoff between the attenuation and source term. Similarly, the two-event data eliminate the ambiguity between the station site response and the attenuation. However, the latter two data sets involve complex event-station geometry (Zhao et al., 2013b), which results in less useful data and makes high-resolution inversion difficult. We compared the attenuation tomography using different data sets. A high-resolution broadband Lg-wave attenuation model for the Middle East and its surrounding regions was obtained by using both data sets.

Given that a survey system is fixed for a data set, the resolution is dependent upon the density of the paths, azimuth coverage, and average path length. To estimate the resolvability at a point, Yanovskaya (1997) defined a criterion based on the radius of the smoothing area, where the radius is approximated by the average value of the two half-axes of the ellipses for a local or regional tomography. This method can provide an analytic resolution evaluation for a dataset, and avoid performing complicated checkerboard tests (Raykova and Panza, 2006). The technique was successfully employed in surface-wave tomography (e.g., Guo et al., 2009; Karagianni et al., 2005; Yanovskaya et al., 2014). Following the procedure proposed by Yanovskaya (1997), we calculated the resolvability radii and obtained horizontal resolution estimates for our tomographic $Q_{Lg}$ maps at individual frequencies.

## 4. Lg-wave attenuation model in the Middle East

Based on the data and method described in the previous sections, we obtained a broadband Lg-wave attenuation model for the Middle East and its adjacent regions. The model is composed of 58 $Q_{Lg}$ distributions at individual frequencies between 0.05 and 10.0 Hz. Simultaneously, the Lg-wave source spectra and station site responses were determined (see Fig. S1 in the supplementary document).

### 4.1. $Q_{Lg}$ maps at individual frequencies

The resultant $Q_{Lg}$ distributions, which are shown in Fig. 3a-c, are overlaid on topography at 0.5, 1.0, and 2.0 Hz, respectively, along with major continental collision sutures (black lines). Correspondingly, Fig. 3d-f show the ray-path coverage (blue lines) and inversion resolutions (red lines). Note that a different color scale is used for each frequency. In the $Q_{Lg}$ maps, the most prominent feature is that the high-frequency $Q_{Lg}$ value is higher than the values at lower frequencies. The lateral $Q_{Lg}$ variations exhibit strong correlations with regional tectonics. Compared with stable continental blocks, e.g., the Eurasian, Arabian, and Indian plates, the continental collision orogenic belt is

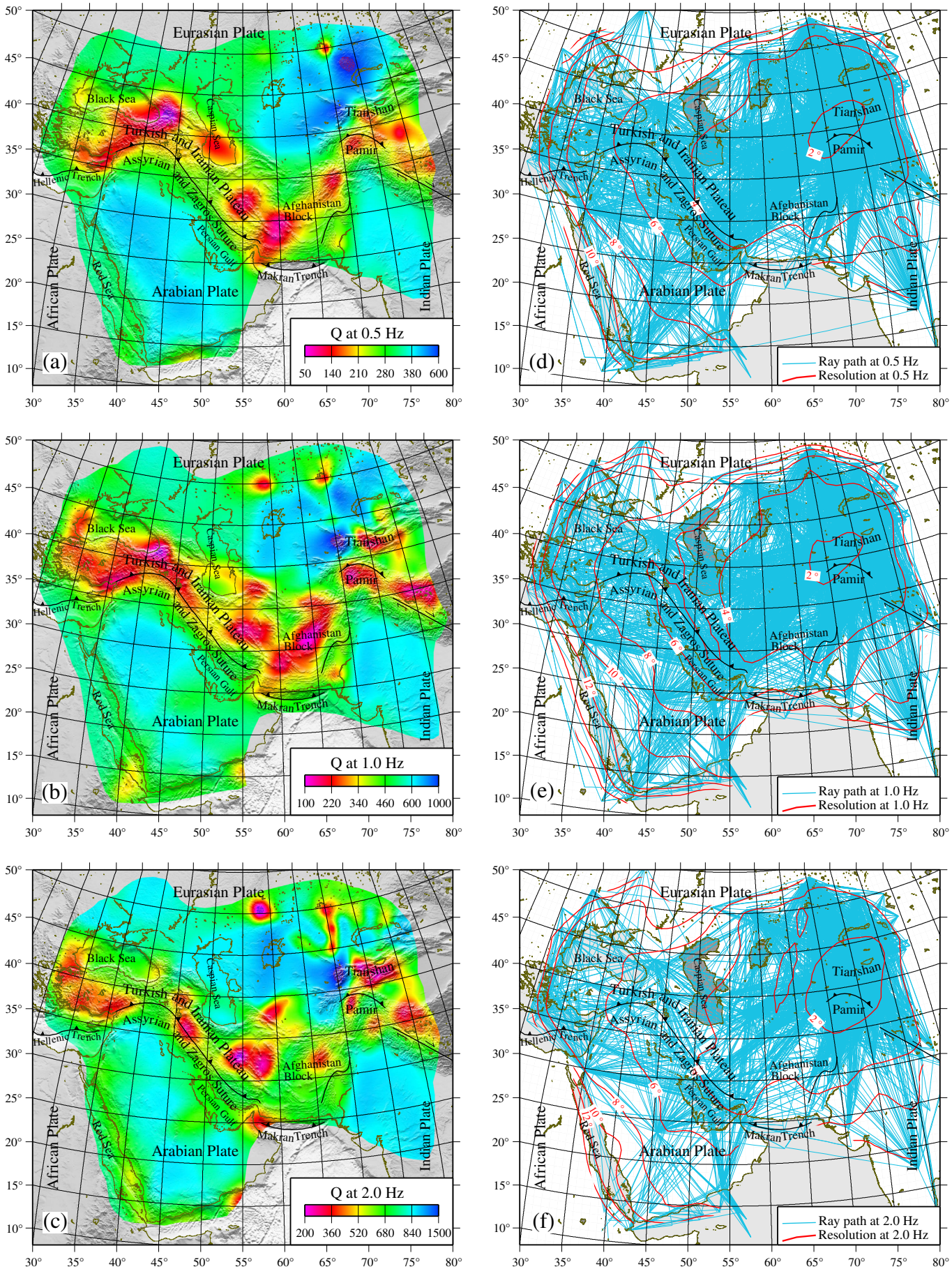
Eurasian Plate
Black Sea
Caspian Sea
Tianshan
Pamir
Turkish and Iranian Plateau
Assyrian and Zagros Suture
Persian Gulf
Hellenic Trench
Afghanistan Block
Makran Trench
Red Sea
African Plate
Arabian Plate
Indian Plate
(a)
Q at 0.5 Hz
50 140 210 280 380 600
(b)
Q at 1.0 Hz
100 220 340 460 600 1000
(c)
Q at 2.0 Hz
200 360 520 680 840 1500
(d)
Ray path at 0.5 Hz
Resolution at 0.5 Hz
(e)
Ray path at 1.0 Hz
Resolution at 1.0 Hz
(f)
Ray path at 2.0 Hz
Resolution at 2.0 Hz

characterized by lower $Q_{Lg}$ values. The low-$Q_{Lg}$ zones arise in the eastern Turkish plateau, central Iran, the Afghanistan block, Pamir, and the Tianshan range, but the specific low-$Q_{Lg}$ zones vary with frequency. For example, the south Caspian Sea is characterized by strong low-frequency attenuation (Fig. 3a), but strong attenuation is not observed at high frequencies (Fig. 3b and c). At individual frequencies the spatial resolution of the tomographic $Q_{Lg}$ maps is estimated using a method for determining the radius of the smoothing area (Yanovskaya, 1997; Yanovskaya et al., 2014). The resolution varies dependent on the data coverage. Regions with high resolution are usually related to high-density ray coverage, evenly distributed ray orientations, and high signal-to-noise ratios. For the frequencies shown in Fig. 3, the average resolution is approximately 6.0° × 6.0°. In the regions where stations are densely distributed, the resolution reaches to 1.5° × 1.5° or higher, which is similar to that obtained with two-station method by Kaviani et al. (2015). Compared to previous studies (e.g., Pasyanos et al., 2009), the resolution in the Arabian Plate is comparable while in regions with dense data coverage, e.g., Tianshan and Pamir regions, the resolutions are much higher. Therefore, investigating attenuation models from different authors, their actual resolutions in different regions and under different frequencies should be considered.

We illustrate the $Q_{Lg}$ distribution at 1 Hz ($Q_0$) to compare our results with previously published Lg attenuation models (Pasyanos et al., 2009; Sandvol et al., 2001; Zor et al., 2007), as shown in Fig. 3b. The dominant features of the crustal attenuation are very similar to previously published results, although the current result has higher resolution. However, certain differences exist. For example, Zor et al. (2007) obtained $Q_0$ values of 250–350 and 670–800 in the northern and southern Arabian platform, respectively, whereas our results indicate $Q_0$ values that vary from 493 to 611 for the entire Arabian plate. In the Afghanistan block, an average $Q_0$ of approximately 262 is obtained, but Pasyanos et al. (2009) estimated $Q_0$ to be 330 in this region. These differences may result from differences in data coverage, inversion resolution, or constraints among individual studies.

As mentioned in the previous section, the Lg-wave attenuation exhibits strong correlations with the regional geology. The $Q_{Lg}$ values change from region to region and vary with individual geology units. Furthermore, the attenuation is strongly dependent on frequency. Therefore the average Lg attenuation tends to be a more robust quantity for characterizing different geological formations (Zhao et al., 2010, 2013a, 2013b). For example, Fig. 4a shows the average process for $Q_{Lg}$ in the continental collision orogenic belt (CC), where light gray crosses indicate tomographically measured $Q_{Lg}$ and circles with error bars denote average $Q_{Lg}$ values within narrow frequency bands defined by $\log_{10}(f_{ref}) \pm 0.15$, where $f_{ref}$ is the reference frequency (Zhao et al., 2010, 2013a, 2013b). The average $Q_0$ value and its standard deviation calculated using logarithm of individual values are also labeled in Fig. 4a. Fig. 4b summarizes the average $Q_{Lg}$ value versus frequency for selected geo-blocks; the red curves are regions from continental collision orogenic zones, whereas the blue curves are related to regions that correspond to stable continental plates. These curves clearly reveal the difference between two types of geological units. The shaded area in Fig. 4b marks the frequency band between 0.2 and 2.0 Hz, within which the $Q_{Lg}$ values are apparently most related to the regional geology. The continental collision orogenic belt has a mean $Q_0$ of 311 (232–417), which is slightly higher than the value of 280 (194–406) found in the Tibetan plateau (Zhao et al., 2013a). However, within the orogenic belt, western blocks have lower $Q_0$ values that are more similar to that of the Tibetan plateau (the Eastern Turkish plateau: 273, Turkish and Iranian plateau: 287, and Afghanistan block: 262), and eastern blocks have relatively higher $Q_0$ values (Pamir plateau: 304 and Tianshan range: 342). The stable continents located in both sides of the orogen are characterized by high $Q_0$ values (The Eurasian plate: 585, Arabian plate: 531, and Indian plate: 571).

### 4.2. Broadband $Q_{Lg}$ images

Fig. 4b shows the frequency dependence of the average $Q_{Lg}$ for selected geo-blocks. $Q_{Lg}$ values between 0.2 and 2.0 Hz exhibit more systematic variations than $Q_{Lg}$ at other frequencies, thus better characterizing the individual geo-blocks. In Fig. 4b, the blue symbols indicate $Q_{Lg}$ values for the stable continental blocks, which are clearly higher than those for the continental collision orogenic zones (red symbols). Also, it appears that the frequency dependence of attenuation within these geo-blocks is not compatible with the commonly used power-law model of $Q_{Lg}$, which is consistent with the results of previous investigations (Pasyanos et al., 2009; Zhao et al., 2010). Therefore, we directly calculated the average $Q_{Lg}$ in logarithmic scale between 0.2 and 2.0 Hz, $Q_{Lg}$ (0.2–2.0 Hz) to extract the broadband property of the crustal attenuation. Like $Q_0$, the $Q_{Lg}$ (0.2–2.0 Hz) is a characteristic value for crustal shear wave attenuation. Most recently, Zhao et al. (2013a) used the $Q_{Lg}$ (0.2–2.0 Hz) anomalies to constrain crustal flow pattern beneath the Tibetan plateau. Fig. 5 shows the broadband $Q_{Lg}$ (0.2–2.0 Hz) image for the Middle East. When compared with the $Q_0$ distribution (Fig. 3b), similar features can be observed in the broadband $Q_{Lg}$ (0.2–2.0 Hz) map, such as the low-$Q_{Lg}$ anomaly regions in the eastern Turkish plateau, central Iran (55°E, 33°N), the Afghanistan block, Pamir, and the Tianshan range. However, some low-frequency low-$Q_{Lg}$ anomalies such as that in south Caspian Sea are also observed in the band-averaged $Q_{Lg}$ (0.2–2.0 Hz) image because of the finite frequency band involved (rather than single frequency involved in $Q_0$). For individual geo-blocks, the $Q_{Lg}$ (0.2–2.0 Hz) values, along with other parameters including the average crustal thickness, $Q_0$ values, Pn velocities, and the block types, are summarized in Table 1.

Using the cross-section images, we investigated the relationships between the frequency dependence of crustal attenuation and regional geology. Three cross-sections for $Q_{Lg}$ versus frequency along two selected latitudes are illustrated in Fig. 6a and b, and a NE–SW cross-section is shown in Fig. 6c. Along each cross-section, the upper part compares the $Q_{Lg}$ (0.2–2.0 Hz), surface topography, and Moho depths from CRUST2.0 (Laske et al., 2013), and the lower part shows $Q_{Lg}$ versus frequency. For each panel, the corresponding longitudes or latitudes are labeled along the top or bottom. The names of major geo-blocks and locations where minimum $Q_{Lg}$ appears (with arrows) are also shown. As shown in Fig. 6a, the 37.5°N section crosses the Eastern Turkish plateau (ET), southern Caspian Sea (CS), Iranian plateau, Eurasian plateau (EP), and Pamir plateau (PA). The Eurasian plateau is a stable continent with high $Q_{Lg}$ values, whereas other geo-blocks in the continental collision orogenic belt tend to have apparently low-$Q_{Lg}$ anomalies. Thick basin sediments may be one cause of the strong attenuation (e.g., Zhao et al., 2010). The southern Caspian sea has low-$Q_{Lg}$ anomalies with an absorbing band between 0.1 and 0.6 Hz, which corresponds to heterogeneity scales between 1.0 and 5.5 km if scattering dominates the observed attenuation (Wu et al., 2000). Shown in Fig. 6b is the 32.5°N section, which passes west to east through the eastern Mediterranean Sea (MS), Arabian plate (AP), Iranian plateau, Afghanistan block (AB), and Indian plate (IP). Two apparent low-$Q_{Lg}$ regions correspond to mountain domains, the Iranian plateau and the AB, whereas the stable continental blocks have relatively higher $Q_{Lg}$ values. At 55°E, 32.5°N, the latitude 32.5°N section (Fig. 6b) and the northeast section (Fig. 6c) exhibit a common low-$Q_{Lg}$ region beneath the Iranian plateau, where Paul et al. (2010) suggested that a mantle collision zone exists between the Arabian and Iranian lithospheres based on a receiver function study.

**Fig. 3.** Selected $Q_{Lg}$ images (a)-(c) and regional maps overlaid with the ray-path coverage and resolution analyses (d)-(f) at 0.5 Hz, 1.0 Hz, and 2.0 Hz, respectively. Note that the major geological faults (black lines) are plotted, and the names of the geo-blocks and thrust faults are labeled.

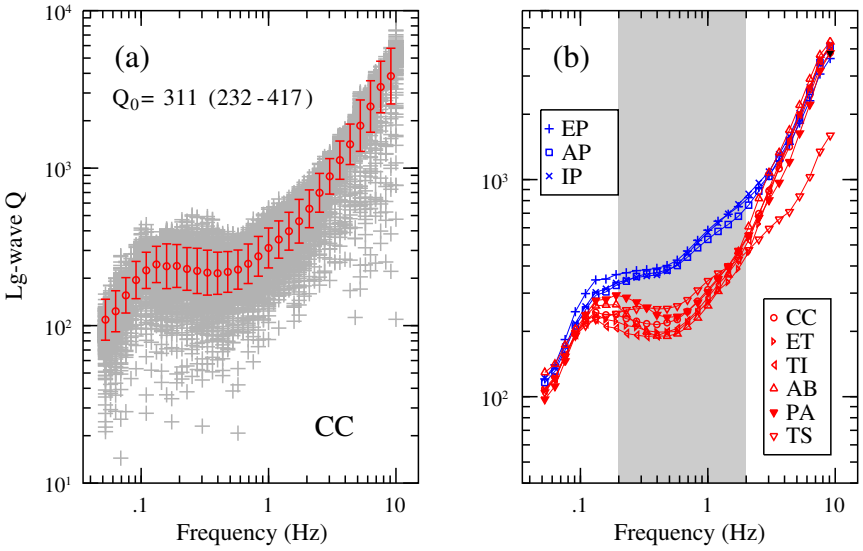


**Fig. 4.** (a) Frequency-dependent $Q_{Lg}$ for the continental collision orogenic belt (CC) and (b) $Q_{Lg}$ versus frequency for different geo-blocks: EP, the Eurasian plate; AP, the Arabian plate; IP, the Indian plate; CC, the continental collision orogenic; ET, the Eastern Turkish plateau; TI, the Turkish and Iranian plateau; AB, the Afghanistan block; PA, the Pamir; and TS, the Tianshan range.

## 5. Strong Lg attenuation in the continental collision orogenic belt

Strong Lg attenuation is observed in the continental collision orogenic zones, whereas the adjacent continental plates show relatively weak attenuation. Fig. 7 compares the crustal attenuation, volcanism, uppermost mantle Pn-velocity, and crustal seismicity within the orogenic belt. The volcanism is obtained from a global volcanism program at http://www.volcano.si.edu/index.cfm, the focal mechanisms are provided by the global Centroid-Moment-Tensor (CMT) project at www.globalcmt.org, and the Pn-velocities are re-plotted from Pei et al. (2011). In Fig. 7a the contours of the broadband $Q_{Lg}$ distribution between 0.2 and 2.0 Hz are shown in white. We also plot the $Q_{Lg}$ contours on the Pn-velocity and seismicity images in Fig. 7b and c for comparison. The Eastern Turkish plateau is characterized by crustal low-$Q_{Lg}$ anomalies, which are consistent with the low-Pn velocities in the uppermost mantle and the volcanic and seismicity activity, thereby suggesting

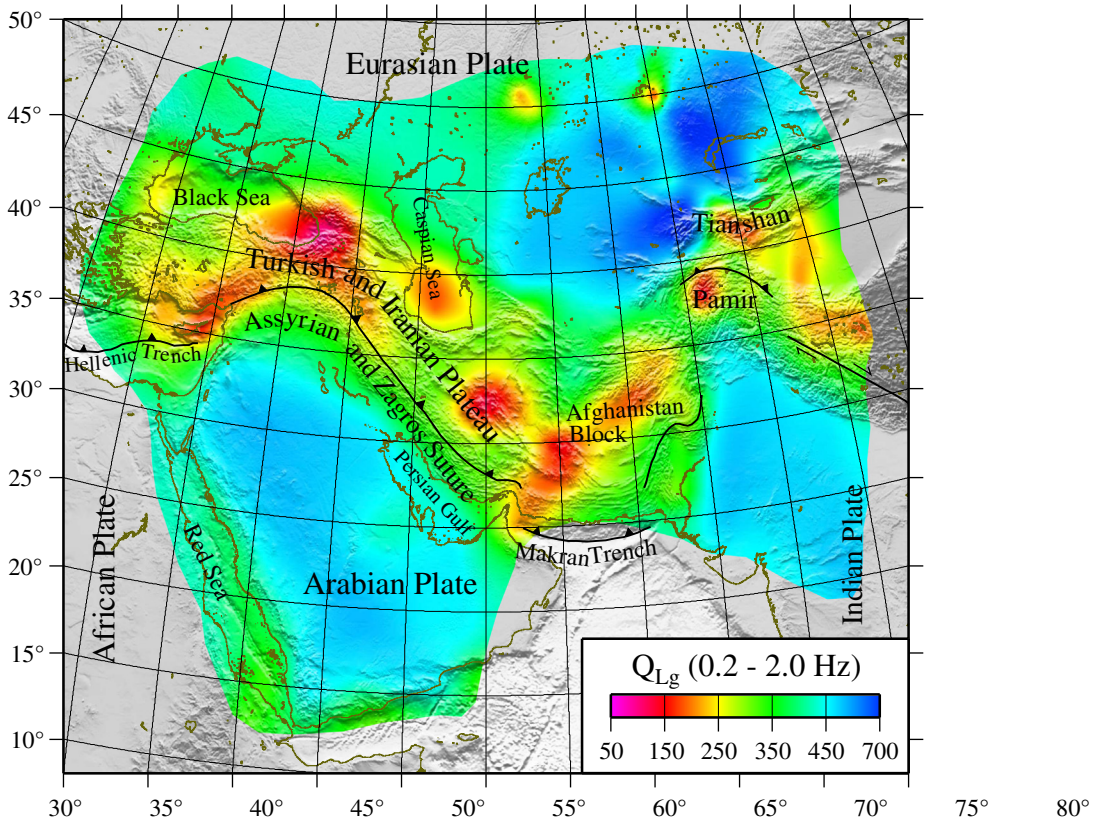


**Fig. 5.** Map that shows an average $Q_{Lg}$ model between 0.2 and 2.0 Hz. Note that the names of geo-blocks and major faults are labeled.

**Table 1**
Lg-wave Q models for individual geo-blocks.

| Geological block | Block name | CRUST2.0 Crustal thickness (km) | $Q_0$ (1 Hz Q) | Broadband Q (0.2 - 2.0 Hz) | Pn velocity (km/s) | Type of blocks |
|---|---|---|---|---|---|---|
| The continental collision orogenic belt | CC | 44.4±9.7 | 311 (232-417) | 270 (182-401) | 8.04±0.15 | Mountains |
| Eurasian plate | EP | 42.8±3.6 | 585 (489-698) | 484 (346-677) | 8.22±0.11 | Plate |
| Arabian plate | AP | 36.0±7.0 | 531 (468-601) | 449 (345-584) | 8.06±0.14 | Plate |
| Indian plate | IP | 38.4±5.4 | 571 (514-635) | 466 (344-631) | 8.18±0.10 | Plate |
| Red sea | RS | 17.0±3.7 | 463 (400-536) | 385 (289-512) | 7.99±0.04 | Basin |
| Mediterranean sea | MS | 26.4±1.7 | 458 (402-521) | 333 (200-554) | 8.15±0.09 | Basin |
| Persian gulf | PG | 38.7±1.4 | 496 (450-546) | 409 (312-536) | 8.23±0.05 | Basin |
| Caspian sea | CS | 40.2±2.7 | 447 (372-537) | 304 (168-549) | 8.16±0.09 | Basin |
| Black sea | BS | 31.9±5.6 | 369 (296-460) | 271 (159-462) | | Basin |
| Eastern Turkish plateau | ET | 39.6±5.7 | 273 (219-341) | 242 (175-334) | 7.90±0.08 | Mountains |
| Turkish and Iranian plateau | TI | 42.5±4.3 | 287 (209-394) | 243 (160-371) | 7.98±0.16 | Mountains |
| Afghanistan block | AB | 41.0±1.9 | 262 (201-343) | 244 (163-364) | 8.05±0.12 | Basin |
| Pamir | PA | 56.0±8.5 | 304 (221-417) | 288 (199-418) | 8.13±0.08 | Mountains |
| Tianshan | TS | 50.2±3.6 | 342 (252-464) | 297 (208-424) | 8.19±0.06 | Mountains |

that in this region, material exchanges between the crust and upper mantle may already have occurred. Partial melting may be widespread in the lower crust, similar to the northern Tibetan plateau (Zhao et al., 2013a; Zor et al., 2007). For the low-$Q_{Lg}$ anomalies in the southern Caspian Sea and central Iranian plateau, corresponding low-Pn velocities or volcanic activity are not observed, thereby suggesting that shallow crustal materials and structures are responsible for the observed low-$Q_{Lg}$ anomalies. For example, thick marine sediments could cause

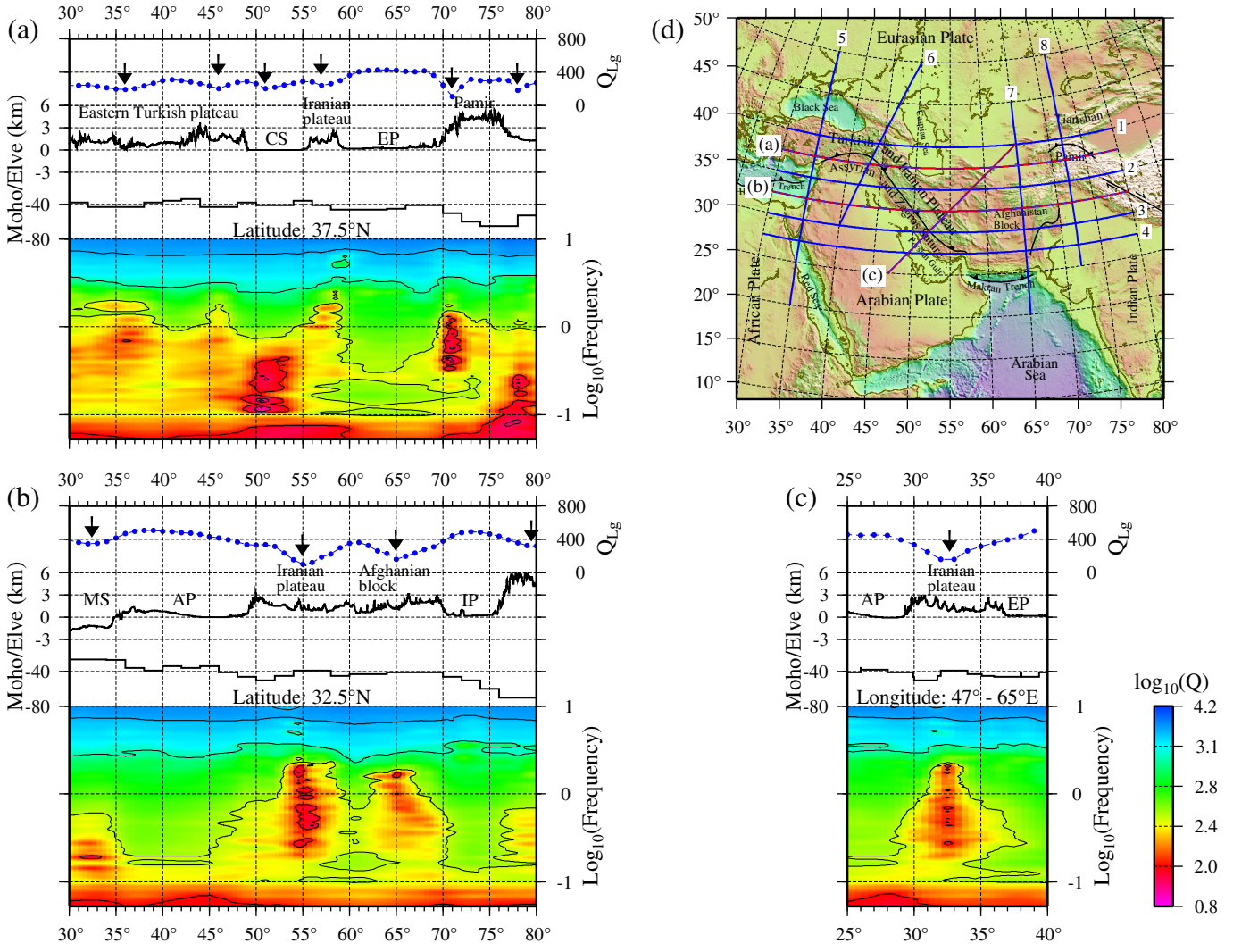


**Fig. 6.** Selected cross-sections of the broadband $Q_{Lg}$ values (a - c) and their surface locations (d), which are indicated by red lines and labeled with corresponding symbols. Upper panel: comparison of the average $Q_{Lg}$, surface topography and Moho depth. Lower panel: $Q_{Lg}$ versus frequency. For (a) and (b), the horizontal coordinate is longitude, and the latitude is labeled in the figures. The cross-section (c) is oriented to the NE and projected onto the NS profile to display the lateral $Q_{Lg}$ variation. The horizontal coordinate is latitude, and the range of longitude variation is labeled in (c). Blue lines that indicate the surface locations for the cross-sections that correspond to the broadband $Q_{Lg}$ values in supplementary Fig. S2 are shown in Fig. 6d.

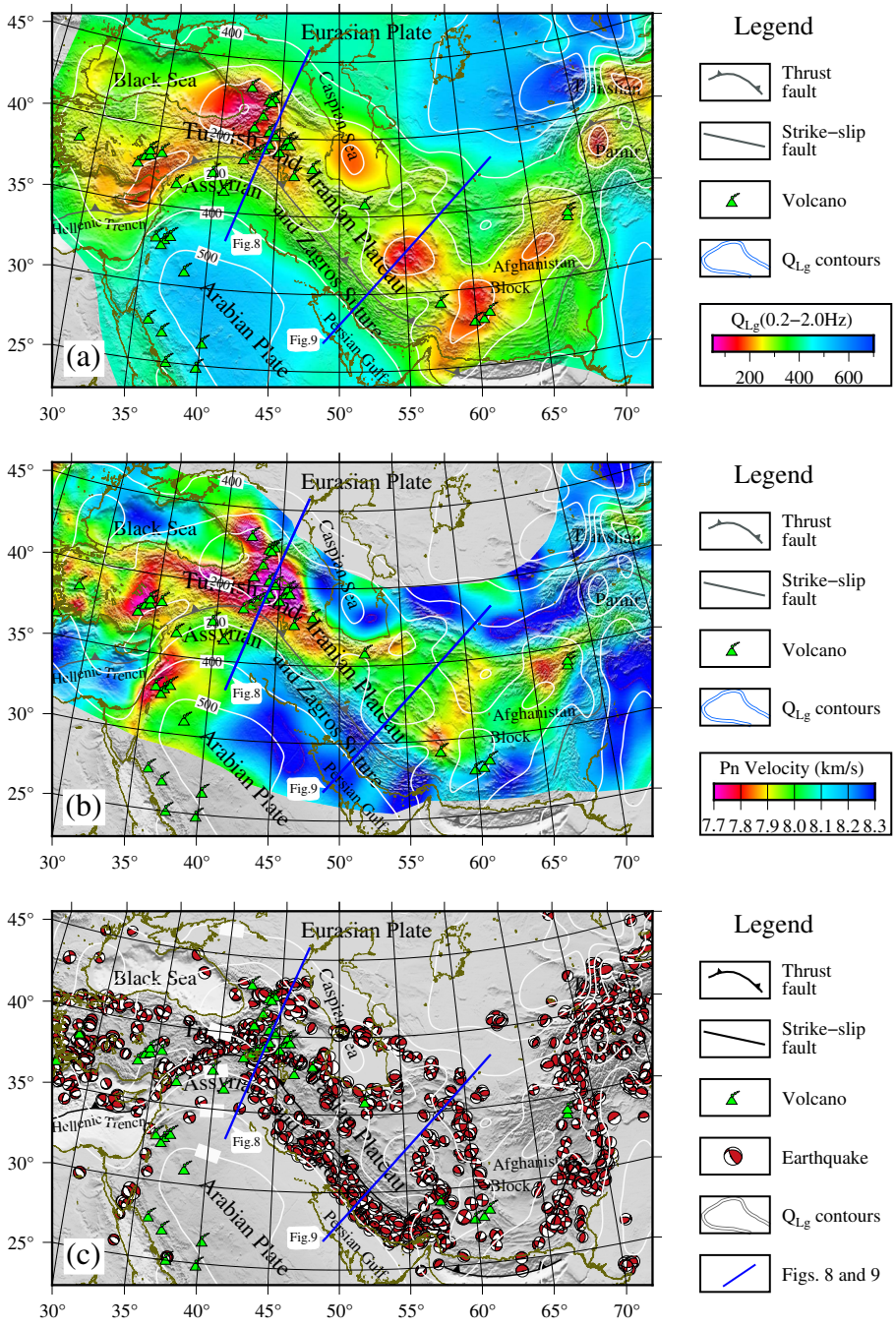


**Fig. 7.** Comparison between (a) the average $Q_{Lg}$ (0.2–2.0 Hz), (b) the Pn velocity, and volcanism overlaid on the figures in the continental collision orogenic belt in the Middle East. Also shown in the figure are major faults (black lines) which indicate the collision boundary, $Q_{Lg}$ contours (white lines), and the names of the geo-blocks. For details, refer to the text.

the strong Lg attenuation in the southern Caspian Sea. The Afghanistan block has a northeast-trending low-$Q_{Lg}$-anomaly belt. The northern part has low-$Q_{Lg}$ anomalies that are in agreement with low-Pn velocities and volcanism. In the southern part, volcanic activity exists, but no low-Pn velocities are observed, thereby suggesting that complex collision processes may have occurred there. The crustal seismicity in the Middle East continental collision belt is shown in Fig. 7c. Many large earthquakes are located in low-$Q_{Lg}$ regions, such as in the Eastern Turkish plateau, and strong $Q_{Lg}$ variation belts, such as the Assyrian and Zagros collision belt. However, there does not seem to be a strong connection between strong Lg attenuation and the seismicity. For example, the south Caspian Sea, central Iranian plateau, and Afghanistan block all have low-$Q_{Lg}$ values but appear to not be seismically active zones.

## 6. Discussion

Compared with the wave speed, seismic attenuation can be more sensitive to the temperature, structure, and presence of fluid phases in the Earth (Solomon, 1972; Wu et al., 2007; Zhang and Lay, 1995). In a continental collision orogenic zone, it is expected that strong Lg attenuation is an indicator of high temperature anomalies or partially molten layers within the crust, and strong $Q_{Lg}$ variation could have geodynamic implications for a continental collision. Therefore, we used two profiles that cross the continental collision zone to compile the surface topography, schematic crust and upper mantle structures, volcanism, seismicity, $Q_{Lg}$ versus frequency distribution, and both $Q_{Lg}$(0.2–2.0 Hz) and Pn velocity variations, with the goal of revealing information regarding

the geodynamics of the continental collision. The locations of the profiles along the surface are indicated by blue lines in Fig. 7.

Fig. 8 shows the profile in the eastern Turkish plateau. It northeastward crosscuts the main faults, where the Bitlis fault (BF), a part of the Assyrian and Zagros suture, is defined as the origin in the relative coordinate system. The Bitlis suture zone (BSZ), an orogenic zone due to continental collision, is located to the south of the BF at the northern margin of the Arabian plate, which we scaled its southwestward extension with negative offsets in our profile. The eastern Turkish plateau (ETP), great Caucasus (GC), and Eurasian plate (Koçyiğit et al., 2001) are located to the north, and all were scaled with positive offsets. As observed from the surface topography shown in Fig. 8a, the orogenic zone spans approximately 800 km. We project the volcanism and earthquakes ($M \geq 2.5$) in range of 2.5° on the schematic crust and upper mantle structures (Fig. 8b). Both volcanism and seismicity appear to cover a broader area than the surface orogenic belt. For the ETP, the high-density earthquakes occurred within the crust (the gray line shows the CRUST2.0 Moho depth), and Plio-Quaternary volcanoes developed there (Kazmin et al., 1986), which may suggest that the strong continental collision in this region resulted in crustal flow and/or partial melting. Beneath the GC, the seismicity extends downward. Moderate-depth earthquakes usually indicate deep Earth dynamic process, such as lithospheric subduction, delamination and/or slab break-off (Argand, 1924). Accordingly, thermal exchange occurred between the crust and uppermost mantle in the orogenic zone and resulted in high-temperature anomalies within the crust; hence, strong Lg attenuation is observed there, as shown in Fig. 8c and d.

Fig. 9 shows the second profile that crosscuts the central Iranian plateau. As a part of the Assyrian and Zagros suture, the main Zagros reverse fault (MZRF) divides the Zagros fold-and-thrust belt (ZFTB) to the south and the Iranian plateau to the north, which correspondingly have negative and positive offsets in the profile, respectively. Recent geological and geophysical observations suggest that the MZRF is deeply rooted, possibly to Moho depths; this rooting appears to be related to the calc-alkaline volcanism of the Sanandaj–Sirjan metamorphic zone (SSZ) and the Urumieh–Dokhtar magmatic arc (UDMA) (Agard et al., 2005; Paul et al., 2006, 2010). Fig. 9b shows the reference Moho depths from CRUST2.0 (gray line), the observed Moho depths (red line) from a receiver function study and inferred traces of the MZRF (blue line) based on gravity data (Paul et al., 2010). An apparent variation of the Moho depths is observed beneath the SSZ, where Paul et al. (2010) suggested a connection zone between Arabian and Iranian lithospheric mantle. In this region, we observe strong Lg attenuation, as shown in Fig. 9c, where the white dashed lines encircle a low-$Q_{Lg}$ area. The low-$Q_{Lg}$ anomaly has an absorbing band between 0.2 and 2.0 Hz, which appears to be similar to the Lg attenuation anomaly observed in the northern Tibetan plateau (Zhao et al., 2013a). Fig. 9d shows that the $Q_{Lg}$ (0.2–2.0 Hz) values correlate very well with the Pn velocities before 300 km and then increase abruptly. The strong crustal attenuation corresponds to the low-Pn velocities the in uppermost mantle, thereby suggesting that the low-$Q_{Lg}$ anomaly may indicate lower crustal partial melting. If the Pn velocity reflects deeper activity compared with crustal attenuation, Fig. 9d may imply that the deep activity extended to further north to the central Iranian plateau domain (CD).

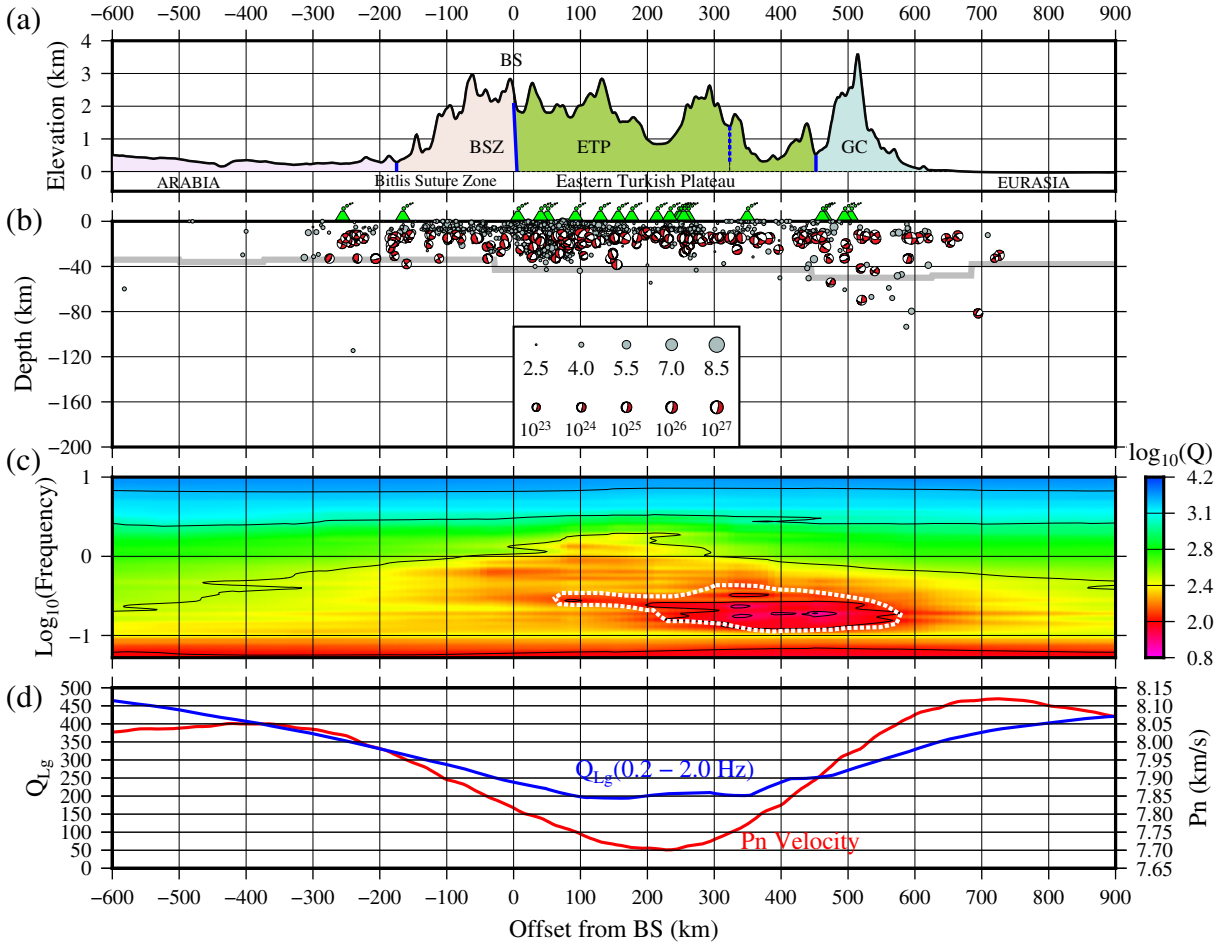


**Fig. 8.** A combined cross-section along the northeastward profile of the eastern Turkish plateau, which is indicated by the blue segments in Fig. 7, with (a) surface topography, (b) volcanism and seismicity in the schematic crust and upper mantle structure, (c) $\log(Q_{Lg})$ versus frequency, and (d) comparison between the average $Q_{Lg}$ and average Pn velocity along the section. For details, refer to the text.

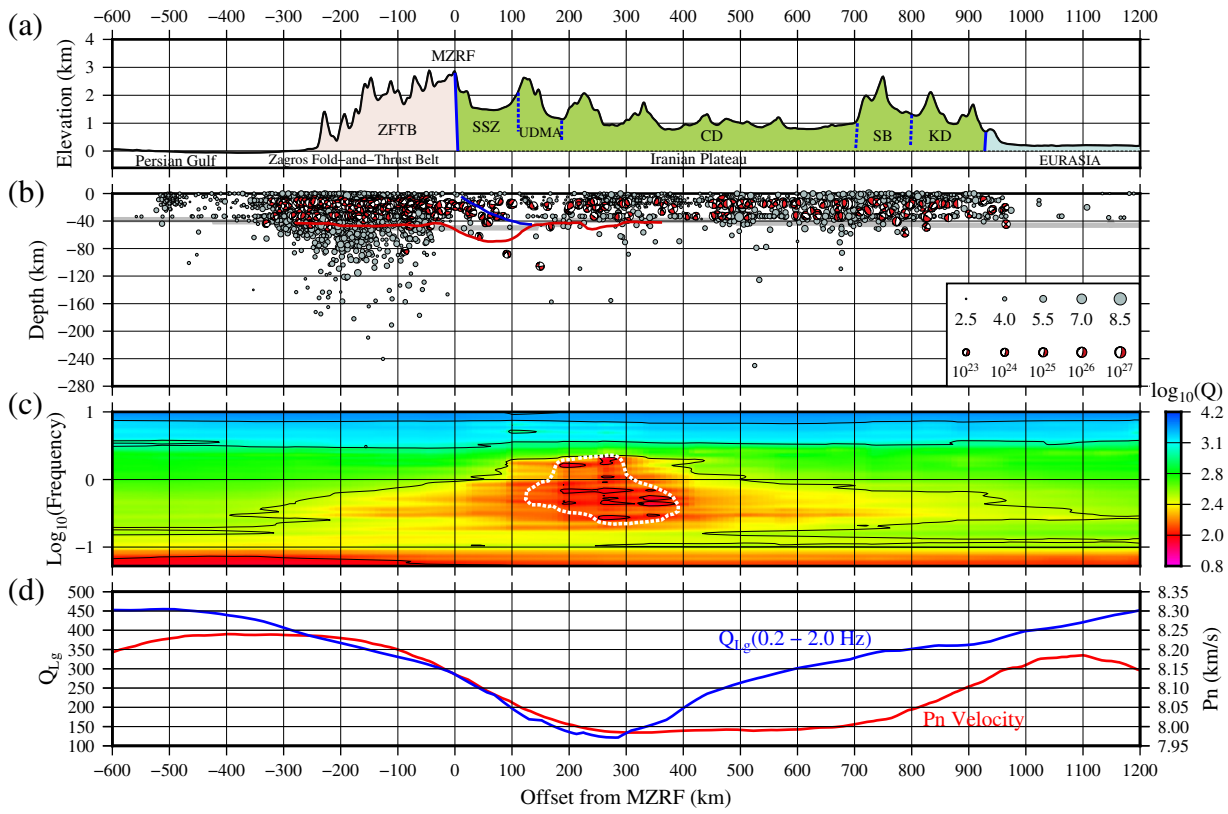


**Fig. 9.** Similar to Fig. 8 but for a combined northeastward cross-section through the central Iranian plateau. For details, refer to the text.

We investigated the relationship between the average low-frequency $Q_{Lg}$ and the average crustal thickness for geological units in the Middle East, and compared them with the data previously obtained for Northeast China, the North China craton, and the Tibetan plateau (Zhao et al., 2010, 2013a, 2013b). The $Q_{Lg}$ versus crustal thickness is illustrated in Fig. 10. The triangles, squares, circles, and diamonds represent the data from different regions, northeastern China (NEC), the north China craton (NCC), the Tibetan plateau (TP) and the Middle East (ME). The TP is characterized by extra-low Q and very thick crust (Fan and Lay, 2002, 2003a, 2003b; Xie, 2002; Xie et al., 2004). The data for stable continental terrains from the NEC, NCC and ME are mostly located at the upper-left of the figure, consistent with the general trend that the $Q_{Lg}$ value increases with increasing crustal thickness, as indicated by the yellow line. For the geo-blocks in the continental collision orogenic belt in the Middle East, the data are apparently located between the stable region data and the active Tibetan data, especially for Pamir (PA), which appears entered into the range of Tibetan data. This result likely indicates that the Middle East orogenic belt is a tectonically active region, although it may not be as active as the Tibetan Plateau. Three major geo-blocks, the Eastern Turkish plateau (ET), the Turkish and Iranian plateau (TI), and the Afghanistan block (AB), are characterized by moderately thick crust of 38 to 44 km and a low average $Q_{Lg}$ value of approximately 220. The plateaus in the Middle East orogenic belt and TP share some similarities in geological structures and geodynamic processes, as has been indicated by many investigators (e.g., Agard et al., 2005; Hatzfeld and Molnar, 2010).

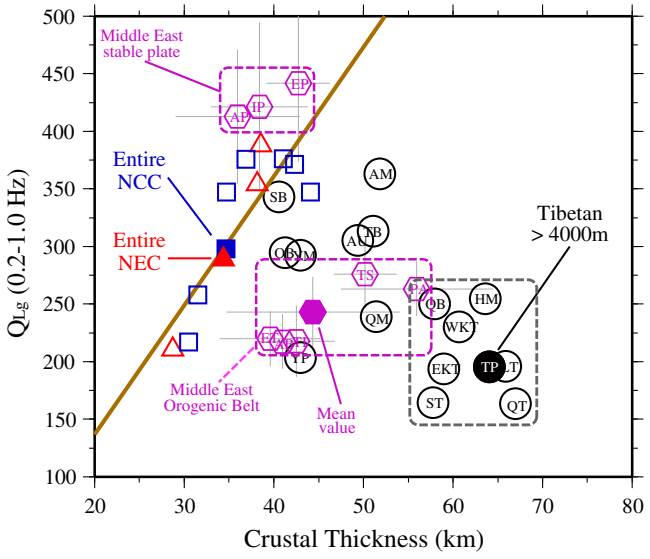


**Fig. 10.** The average $Q_{Lg}$ value versus the average crustal thickness for selected geology units in mainland China (NEC: red triangles; NCC: blue squares; and TP: black circles) and the Middle East (ME: pink diamonds). Note that the Middle East data are encircled by pink dashed lines and are clearly divided into two groups, the stable continental plate group and the orogenic belt terrain population. For details, refer to the text.

## 7. Conclusions

We developed a 0.05–10.0 Hz broadband Lg-wave attenuation model for the Middle East. By simultaneously considering the ray-path density, azimuth coverage, and average ray-path length, we used an analytic method (Yanovskaya, 1997; Yanovskaya et al., 2014) to evaluate the tomographic resolution. The average resolution of our broadband Lg-wave attenuation model is approximately 6.0° × 6.0°. Because of the multiple datasets (including the single-station, two-station, and two-event data) and the joint inversion scheme (Zhao et al., 2013b) used, the resulting attenuation model has a higher resolution than previous results from two-station measurements. Strong Lg attenuation is observed in the Middle East continental collision orogenic belt. Both tectonic complexity and widespread crustal melting are likely to be responsible for the low-$Q_{Lg}$ anomalies in the continental collision zone,

and their possible causes of strong attenuation characteristics seem to be agreement with those in the Tibetan plateau. In the eastern Turkish plateau, low-$Q_{Lg}$ anomalies, low-Pn velocities (Pei et al., 2011), strong volcanic activity, complex seismicity and GPS velocity (Hatzfeld and Molnar, 2010), are consistent with the interpretation in terms of current continental collision, and suggest possible crustal partial melting occurred there and that both high topography and lateral extrusion drive the westward flow of crustal materials.

## Acknowledgments

We thank Profs. Thorne Lay, Zhen-Xing Yao, James Ni and Xiao-Bo Tian, Drs. Jiakang Xie, Xiaoning Yang, Bo Wan and Na Fan for many discussions and comments on this work. We also thank the Editor J.-P. Avouac and an anonymous reviewer for their helpful and constructive comments. The broadband data used in this study were retrieved from the IRIS Data Management Center and the NEIC. The Pn velocities used in Fig. 7b were provided by Dr. S. Pei (Pei et al., 2011). Some figures are created using GMT (Wessel and Smith, 1998). This research was supported by the National Natural Science Foundation of China (grants 41374065 and 41174048). X.B. Xie wishes to thank AFRL for support under grant FA9453-12-C-0234.

## Appendix A. Lg-wave spectral amplitudes

### A.1. Single-station data

At a given frequency $f$, the observed Lg-wave spectral amplitude $A$ recorded at station $i$ from event $k$ can be expressed as

$$A_{ki} = S_k G_{ki} \Gamma_{ki} P_i R_{ki}, \tag{A1}$$

where $S_k$ is the source term, $G_{ki} = (\Delta_0 \Delta_{ki})^{-1/2}$ is the geometrical spreading proposed by Street et al. (1975) and adopted by many investigators (e.g., Pasyanos et al., 2009; Xie, 1993; Zhao et al., 2010, 2013b), $\Delta_{ki} \geq 100$ km is the epicentral distance between the source and the station, and $\Delta_0$ is a reference distance that is fixed to 100 km. The attenuation term can be expressed as

$$\Gamma_{ki} = \exp\left[-\frac{\pi f}{V} \cdot \int_k^i \frac{ds}{Q(x,y,f)}\right], \tag{A2}$$

where $V$ is the mean Lg-wave group velocity, $\int_k^i ds$ is the integral along the great circle ray path from the source to station, and $Q(x,y,f)$ is the Lg-wave quality factor, which is a function of the frequency and the surface location $(x,y)$. $P_i$ is the frequency-dependent site response due to the local Earth structures. The factor $R_{ki}$ denotes unexplained propagation effects that are usually neglected in computations (e.g., Xie, 1993; Zhao et al., 2010, 2013b).

### A.2. Two-station and two-event data

If two stations record the same earthquake within a narrow azimuthal range, by assuming the source and two stations are approximately aligned, we can eliminate the source term to obtain two-station data (e.g., Bao et al., 2011a; Xie et al., 2004; Zhao et al., 2010, 2013b). For this purpose, a maximum azimuth range of 15° was chosen by Xie et al. (2004) to screen the two-station data, whereas Zhao et al. (2013b) used another criterion, which requires that the distance from the near station to the ray path of the far station be less than half the grid spacing. Under this circumstance, the interstation amplitude can be calculated as (refer to Fig. 4 in Zhao et al., 2013b).

$$A_{lj} \approx \frac{A_{kj}}{A_{ki}} = \left(\frac{\Delta_{kj}}{\Delta_{ki}}\right)^{-1/2} \cdot \exp\left[-\frac{\pi f}{V} \cdot \left(\int_l^j \frac{ds}{Q(x,y,f)}\right)\right] \cdot \frac{P_j}{P_i}, \tag{A3}$$

where $A_{ki}$ and $A_{kj}$ are the spectral amplitudes recorded by stations $i$ and $j$ for event $k$ and $l$ is a reference point on the ray-path $kj$. Similarly, the two-event amplitude can be calculated as

$$A_{lj} \approx \frac{A_{jk}}{A_{ik}} = \frac{S_j}{S_i} \cdot \left(\frac{\Delta_{jk}}{\Delta_{ik}}\right)^{-1/2} \cdot \exp\left[-\frac{\pi f}{V} \cdot \left(\int_l^j \frac{ds}{Q(x,y,f)}\right)\right], \tag{A4}$$

where $A_{jk}$ and $A_{ik}$ are spectral amplitudes from events $i$ and $j$ recorded at the same station $k$ and $l$ is a reference point on the ray-path $jk$.

## Appendix B. Supplementary data

Supplementary data to this article can be found online at http://dx.doi.org/10.1016/j.tecto.2016.02.025.

## References

Agard, P., Omrani, J., Jolivet, L., Mouthereau, F., 2005. Convergence history across Zagros (Iran): constraints from collisional and earlier deformation. Int. J. Earth Sci. 94, 401–419.
Aki, K., Chouet, B., 1975. Origin of coda waves: source, attenuation, and scattering effects. J. Geophys. Res. 80, 3322–3342.
Akinci, A., Ibáñez, J.M., Delpezzo, E., Morales, J., 1995. Geometrical spreading and attenuation of Lg waves: a comparison between western Anatolia (Turkey) and southern Spain. Tectonophysics 250, 47–60.
Al-Damegh, K., Sandvol, E., Al-Lazki, A., Barazangi, M., 2004. Regional seismic wave propagation (Lg and Sn) and Pn attenuation in the Arabian Plate and surrounding regions. Geophys. J. Int. 157, 775–795.
Allen, M.B., Armstrong, H.A., 2008. Arabia-Eurasia collision and the forcing of mid-Cenozoic global cooling. Palaeogeogr. Palaeoclimatol. Palaeoecol. 265, 52–58.
Argand, E., 1924. La tectonique de l'Asie. Congr. Géol. Int. Liège 1922, 169–371.
Bao, X.Y., Sandvol, E., Ni, J., Hearn, T., Chen, Y.S.J., Shen, Y., 2011a. High resolution regional seismic attenuation tomography in eastern Tibetan Plateau and adjacent regions. Geophys. Res. Lett. 38, L16304.
Bao, X.Y., Sandvol, E., Zor, E., Sakin, S., Mohamad, R., Gök, R., Mellors, R., Godoladze, T., Yetirmishli, G., Turkelli, N., 2011b. Pg attenuation tomography within the northern Middle East. Bull. Seismol. Soc. Am. 101, 1496–1506.
Benz, H.M., Frankel, A., Boore, D.M., 1997. Regional Lg attenuation for the continental United States. Bull. Seismol. Soc. Am. 87, 606–619.
Berberian, M., King, G.C.P., 1981. Towards a paleogeogrpahy and tectonic evolution of Iran. Can. J. Earth Sci. 18, 210–265.
Chun, K.Y., West, G.F., Kokoski, R.J., Samson, C., 1987. A novel technique for measuring Lg attenuation — results from eastern Canada between 1 to 10 Hz. Bull. Seismol. Soc. Am. 77, 398–419.
Cong, L.L., Mitchell, B.J., 1998. Lg coda Q and its relation to the geology and tectonics of the Middle East. Pure Appl. Geophys. 153, 563–585.
Copley, A., McKenzie, D., 2007. Models of crustal flow in the India-Asia collision zone. Geophys. J. Int. 169, 683–698.
Dewey, J.F., Hempton, M.R., Kidd, W.S.F., Saroglu, F., Sengör, A.M.C., 1986. Shortening of Continental Lithosphere: the Neotectonics of Eastern Anatolia — a Young Collision Zone. In: Coward, M.P., Ries, A.C. (Eds.), Collision Tectonics. Geological Society, London, Special Publications, London, pp. 3–36.
Fan, G.W., Lay, T., 2002. Characteristics of Lg attenuation in the Tibetan plateau. J. Geophys. Res. 107 (B10), 2256.
Fan, G.W., Lay, T., 2003a. Strong Lg attenuation in the Tibetan plateau. Bull. Seismol. Soc. Am. 93, 2264–2272.
Fan, G.W., Lay, T., 2003b. Strong Lg wave attenuation in the northern and eastern Tibetan plateau measured by a two-station/two-event stacking method. Geophys. Res. Lett. 30 (10), 1530.
Ford, S.R., Dreger, D.S., Mayeda, K., Walter, W.R., Malagnini, L., Phillips, W.S., 2008. Regional attenuation in Northern California: A comparison of five 1D Q methods. Bull. Seismol. Soc. Am. 98, 2033–2046.
Gök, R., Sandvol, E., Türkelli, N., Seber, D., Barazangi, M., 2003. Sn attenuation in the Anatolian and Iranian plateau and surrounding regions. Geophys. Res. Lett. 30, 8042.
Guo, Z., Gao, X., Yao, H.J., Li, J., Wang, W.M., 2009. Midcrustal low-velocity layer beneath the central Himalaya and southern Tibet revealed by ambient noise array tomography. Geochem. Geophys. Geosyst. 10.
Hatzfeld, D., Molnar, P., 2010. Comparisons of the kinematics and deep structures of the Zagros and Himalaya and of the Iranian and Tibetan plateaus and geodynamic implications. Rev. Geophys. 48.
Jolivet, L., Faccenna, C., 2000. Mediterranean extension and the Africa–Eurasia collision. Tectonics 19, 1095–1106.
Kadinsky-Cade, K., Barazangi, M., Oliver, J., Isacks, B., 1981. Lateral variations of high-frequency seismic-wave propagation at regional distances across the Turkish and Iranian plateaus. J. Geophys. Res. 86, 9377–9396.
Karagianni, E.E., Papazachos, C.B., Panagiotopoulos, D.G., Suhadolc, P., Vuan, A., Panza, G.F., 2005. Shear velocity structure in the Aegean area obtained by inversion of Rayleigh waves. Geophys. J. Int. 160, 127–143.
Kaviani, A., Sandvol, E., Bao, X.Y., Rumpker, G., Gök, R., 2015. The structure of the crust in the Turkish-Iranian plateau and Zagros using Lg Q and velocity. Geophys. J. Int. 200, 1252–1266.

Kazmin, V.G., Sbortshikov, I.M., Ricou, L.E., Zonenshain, L.P., Boulin, J., Knipper, A.L., 1986. Volcanic belts as markers of the Mesozoic–Cenozoic active margin of Eurasia. Tectonophysics 123, 123–152.
Koçyiğit, A., Yilmaz, A., Adamia, S., Kuloshvili, S., 2001. Neotectonics of east Anatolian plateau (Turkey) and Lesser Caucasus: implication for transition from thrusting to strike-slip faulting. Geodin. Acta 14, 177–195.
Laske, G., Masters, G., Ma, Z., Pasyanos, M., 2013. Update on CRUST1.0 — a 1-degree global model of Earth's crust. Geophys. Res. Abstr. 15 (Abstract EGU2013-2658).
McNamara, D.E., Walter, W.R., 2001. Mapping crustal heterogeneity using Lg propagation efficiency throughout the Middle East, Mediterranean, Southern Europe and Northern Africa. Pure Appl. Geophys. 158, 1165–1188.
Mitchell, B.J., Pan, Y., Xie, J.K., Cong, L.L., 1997. Lg coda Q variation across Eurasia and its relation to crustal evolution. J. Geophys. Res. 102, 22767–22779.
Mitchell, B.J., Cong, L.L., Ekstrom, G., 2008. A continent-wide map of 1-Hz Lg coda Q variation across Eurasia and its relation to lithospheric evolution. J. Geophys. Res. 113, B04303.
Pasyanos, M.E., Matzel, E.M., Walter, W.R., Rodgers, A.J., 2009. Broad-band Lg attenuation modelling in the Middle East. Geophys. J. Int. 177, 1166–1176.
Paul, A., Kaviani, A., Hatzfeld, D., Vergne, J., Mokhtari, M., 2006. Seismological evidence for crustal-scale thrusting in the Zagros mountain belt (Iran). Geophys. J. Int. 166, 227–237.
Paul, A., Hatzfeld, D., Kaviani, A., Tatar, M., Pequegnat, C., 2010. Seismic imaging of the lithospheric structure of the Zagros mountain belt (Iran). In: Leturmy, P., Robin, C. (Eds.), Tectonic and stratigraphic evolution of Zagros and Makran during the Mesozoic-Cenozoic vol. 330. Geol. Soc. London, Special Publications, pp. 5–18.
Pei, S.P., Zhao, J.M., Rowe, C.A., Wang, S.Y., Hearn, T.M., Xu, Z.H., Liu, H.B., Sun, Y.S., 2006. $M_L$ amplitude tomography in North China. Bull. Seismol. Soc. Am. 96, 1560–1566.
Pei, S.P., Sun, Y.S., Toksoz, M.N., 2011. Tomographic Pn and Sn velocity beneath the continental collision zone from Alps to Himalaya. J. Geophys. Res. 116, B10311.
Phillips, W.S., Hartse, H.E., Rutledge, J.T., 2005. Amplitude ratio tomography for regional phase Q. Geophys. Res. Lett. 32.
Rahimi, H., Motaghi, K., Mukhopadhyay, S., Hamzehloo, H., 2010. Variation of coda wave attenuation in the Alborz region and Central Iran. Geophys. J. Int. 181, 1643–1654.
Ranasinghe, N.R., Gallegos, A.C., Trujillo, A.R., Blanchette, A.R., Sandvol, E.A., Ni, J., Hearn, T.M., Tang, Y.C., Grand, S.P., Niu, F.L., Chen, Y.S.J., Ning, J.Y., Kawakatsu, H., Tanaka, S., Obayashi, M., 2015. Lg attenuation in northeast China using NECESSArray data. Geophys. J. Int. 200, 67–76.
Raykova, R.B., Panza, G.F., 2006. Surface waves tomography and non-linear inversion in the southeast Carpathians. Phys. Earth Planet. Inter. 157, 164–180.
Rodgers, A.J., Ni, J.F., Hearn, T.M., 1997. Propagation characteristics of short-period Sn and Lg in the Middle East. Bull. Seismol. Soc. Am. 87, 396–413.
Sandvol, E., Al-Damegh, K., Calvert, A., Seber, D., Barazangi, M., Mohamad, R., Gok, R., Turkelli, N., Gurbuz, C., 2001. Tomographic imaging of Lg and Sn propagation in the Middle East. Pure Appl. Geophys. 158, 1121–1163.
Sengör, A.M.C., Kidd, W.S.F., 1979. Post-collisional tectonics of the Turkish-Iranian plateau and a comparison with Tibet. Tectonophysics 55, 361–376.
Solomon, S.C., 1972. Seismic-wave attenuation and partial melting in the upper mantle of North America. J. Geophys. Res. 77, 1483–1502.
Stampfli, G.M., 2000. Tethyan oceans. J. Geol. Soc. Lond. 173, 1–23.
Street, R.L., Herrmann, R.B., Nuttli, O.W., 1975. Spectral characteristics of Lg wave generated by central United States earthquakes. Geophys. J. R. Astron. Soc. 41 (51-&).
Vanderhaeghe, O., Teyssier, C., 2001. Partial melting and flow of orogens. Tectonophysics 342, 451–472.
Wessel, P., Smith, W., 1998. New, improved version of the generic mapping tools released. Eos 79, 579.
Wu, R.S., Jin, S., Xie, X.B., 2000. Energy partition and attenuation of Lg waves by numerical simulations using screen propagators. Phys. Earth Planet. Inter. 120, 227–243.
Wu, R.S., Wu, X.Y., Xie, X.B., 2007. Simulation of high-frequency wave propagation in complex crustal waveguides using generalized screen propagators. Adv. Geophys. 48, 323–363.
Xie, J., 1993. Simultaneous inversion for source spectrum and path-Q using Lg with application to 3 Semipalatinsk explosions. Bull. Seismol. Soc. Am. 83, 1547–1562.
Xie, J., 2002. Lg Q in the eastern Tibetan plateau. Bull. Seismol. Soc. Am. 92, 871–876.
Xie, J., Mitchell, B.J., 1990. Attenuation of multiphase surface waves in the basin and range province, part I: Lg and Lg coda. Geophys. J. Int. 102, 121–137.
Xie, J., Gök, R., Ni, J., Aoki, Y., 2004. Lateral variations of crustal seismic attenuation along the INDEPTH profiles in Tibet from Lg Q inversion. J. Geophys. Res. 109, B10308.
Xie, J., Wu, Z., Liu, R., Schaff, D., Liu, Y., Liang, J., 2006. Tomographic regionalization of crustal Lg Q in eastern Eurasia. Geophys. Res. Lett. 33, L03315.
Yanovskaya, T.B., 1997. Resolution estimation in the problems of seismic ray tomography. Izv. Phys. Solid Earth 33, 76–80.
Yanovskaya, T.B., Lyskova, E.L., Koroleva, T.Y., 2014. The velocity structure of the Carpathian zone from the ambient noise surface wave tomography. Izv. Phys. Solid Earth 50, 632–640.
Yin, A., 2010. Cenozoic tectonic evolution of Asia: A preliminary synthesis. Tectonophysics 488, 293–325.
Yin, A., Harrison, T.M., 2000. Geologic evolution of the Himalayan-Tibetan orogen. Annu. Rev. Earth Planet. Sci. 28, 211–280.
Yin, A., Rumelhart, P.E., Butler, R., Cowgill, E., Harrison, T.M., Foster, D.A., Ingersoll, R.V., Zhang, Q., Zhou, X.Q., Wang, X.F., Hanson, A., Raza, A., 2002. Tectonic history of the Altyn Tagh fault system in northern Tibet inferred from Cenozoic sedimentation. Geol. Soc. Am. Bull. 114, 1257–1295.
Zhang, T.R., Lay, T., 1995. Why the Lg phase does not traverse oceanic crust. Bull. Seismol. Soc. Am. 85, 1665–1678.
Zhao, L.F., Xie, X.B., Wang, W.M., Zhang, J.H., Yao, Z.X., 2010. Seismic Lg-wave Q tomography in and around Northeast China. J. Geophys. Res. 115, B08307.
Zhao, L.F., Xie, X.B., He, J.K., Tian, X.B., Yao, Z.X., 2013a. Crustal flow pattern beneath the Tibetan plateau constrained by regional Lg-wave Q tomography. Earth Planet. Sci. Lett. 383, 113–122.
Zhao, L.F., Xie, X.B., Wang, W.M., Zhang, J.H., Yao, Z.X., 2013b. Crustal Lg attenuation within the North China craton and its surrounding regions. Geophys. J. Int. 195, 513–531.
Zor, E., Sandvol, E., Xie, J.K., Turkelli, N., Mitchell, B., Gasanov, A.H., Yetirmishli, G., 2007. Crustal attenuation within the Turkish plateau and surrounding regions. Bull. Seismol. Soc. Am. 97, 151–161.